Journal of
Nanoscience and Nanotechnology
Vol. 11, 7802–7806, 2011

The Morphology-Dependent Photocatalysis for Rhodamine B Degradation Over Bi_2WO_6 Hierarchical Nanostructure

Yue Tian, Ming Fang, Wei Xu, Nian Li, Yongzhou Chen, and Lide Zhang*

Key Lab of Materials Physics, Anhui Key laboratory of Nanomaterials and Nanostructure, Institute of Solid State Physics, Chinese Academy of Sciences, Hefei, 230031, P. R. China

In this paper, the nanostructured Bi_2WO_6 with different hierarchical morphologies was synthesized via a warmly hydrothermal route. The structure and morphology of the as-prepared Bi_2WO_6 products were characterized by X-ray diffraction (XRD), field emission scanning electron microscope (FE-SEM), UV-vis absorption spectroscopy (UV-Vis) and N_2-sorption analysis. The photocatalytic efficiency of Bi_2WO_6 was investigated by photodegradation of rhodamine B (RhB) under visible-light irradiation. The present work demonstrated that Bi_2WO_6 with four different hierarchical structures was effective visible-light-driven photocatalytic functional material for environmental purification. Moreover, the nest-like Bi_2WO_6 exhibited superior photocatalytic effects on rhodamine B degradation compared with other three Bi_2WO_6 morphologies. The excellent catalytic effect of the nest-like Bi_2WO_6 was attributed to its unique structural property and large surface area. The relationship between morphology and photocatalytic performance was discussed in detail. The photocatalytic mechanism for the degradation of RhB was also investigated, which revealed the important role of morphology in improving the photocatalyitc activities of Bi_2WO_6.

Keywords: Bi_2WO_6, Nanomaterials, Morphology, Visible Light, Photocatalysis.

RESEARCH ARTICLE

1. INTRODUCTION

In recent years, a large number of investigations have been focused on the semiconductor-based photocatalysts because of their wide potential applications in solar energy conversion and environmental purification.[1–2] In view of the efficient utilization of visible light, which accounts for a large proportion of the solar spectrum, the discovery of an active visible-light-driven photocatalyst often attracts much attention.[3–5] Perovskite structured Bi_2WO_6 (BWO) has been reported as one of the most promising visible-light-driven photocatalysts when used to decompose water dyes and indoor pollutants.[6–8] Although considerable efforts have been devoted to reveal its unique physical and chemical properties, there are few reports on the relationship between the properties and the synthesized morphology of Bi_2WO_6. Thereby, it is urgent to further explore the structure, morphology and application of this new photocatalyst.

Generally, the properties of materials are greatly depended on their structures including compositions, crystal structure and microstructure.[9–11] Especially for photocatalysts, the most important factors determining the activity are considered to be surface area and structural properties such as crystalline quality, particle size, size distribution, band gap energy, etc.[12] So, the morphology of the catalyst, which determines both surface area and the structural properties mentioned above, plays an important role in the catalytic activity. Morphology-tunable synthesis of inorganic materials via simple methods is of great interest in many fields.[13–15] Recently, we have reported directed growth of Bi_2WO_6 hierarchical nano/microstructures with different morphologies using a surfactant-assisted hydrothermal route.[16] These hierarchical nano/microstructures possess large specific surface areas, which facilitate efficient contact of photocatalysts with organic contaminants and increase the active sites for photocatalytic reactions.

In this work, we focus our attention on evaluating the morphology-dependent photocatalytic effects of these hierarchical nanostructured Bi_2WO_6, using the photocatalytic degradation of rhodamine B (RhB) as the model reaction. The degradability and degradation kinetics for the Bi_2WO_6 products were evaluated. The relationship

*Author to whom correspondence should be addressed.

 1533-4880/2011/11/7802/005 doi:10.1166/jnn.2011.4740

between morphology and photocatalytic activity was discussed to understand the reaction pathways.

2. EXPERIMENTAL DETAILS

2.1. Catalysts Preparation

Bi_2WO_6 was synthesized using a hydrothermal method, all of the agents used were of AR grade. In a typical synthesis process, 1.2 g $Bi(NO_3)_3 \cdot 5H_2O$ with surfactant cetyltrimethyl ammonium bromide (CTAB) was first dissolved in a nitric acid solution (1.0 mol L^{-1}, 10 mL) to avoid hydrolysis of Bi^{3+} ions, then the solution was magnetically stirred at room temperature for 30 min. A white precipitate was formed when 0.4 g $Na_2WO_4 \cdot 2H_2O$ was added into the above solution. The pH values of the suspensions were adjusted to 0.5, 2.0, 4.0 and 7.0 by adding NaOH solution (4 mol L^{-1}), respectively. After being stirred for 60 min, the suspension was added to a 60 mL Teflon-lined autoclave up to 80% of the total volume. Then, the autoclave was sealed in a stainless steel tank and heated at 180 °C for 20 h. Subsequently, the reactor was cooled to room temperature naturally. The obtained samples were collected and washed with de-ionized water and dried at 80 °C in air.

2.2. Characterization

XRD patterns were recorded with a Philips X'pert powder X-ray diffractometer with Cu Kα (0.15419 nm) radiation. The Scanning Electron Microscopy (SEM) was performed on a Sirion 200 field emission scanning electron microscope. The optical diffuse reflectance spectra were conducted on a UV-vis spectrophotometer (Hitachi U-3010). Nitrogen adsorption–desorption measurements were conducted at 77.35 K on a Micromeritics Tristar 3000 analyzer. The BET surface area was estimated using adsorption data.

2.3. Photocatalytic Tests

Photocatalytic activity was evaluated by the degradation of RhB under visible-light irradiation using a 300 W Xe lamp with a cutoff filter ($\lambda > 400$ nm). In each experiment, photocatalyst powders (0.2 g) were added into RhB solution (1×10^{-5} M, 100 mL). Before illumination, the suspensions were magnetically stirred in darkness for 60 min to establish an adsorption/desorption equilibrium between photocatalyst powders and RhB. At different irradiation time intervals, about 5 mL solutions were collected, and then centrifugalized to remove the photocatalysts. The concentrations of the remnant RhB were monitored by UV-vis spectroscopy at 553 nm.

3. RESULTS AND DISCUSSION

3.1. Characterization of Catalysts

Figure 1 shows the overall morphologies of Bi_2WO_6 products. Various shapes of Bi_2WO_6 are obtained by changing the pH value of the precursor solutions. The Bi_2WO_6 crystals synthesized in the solution with pH 7.0 show a lamella-shaped morphology (Fig. 1(a)). The Bi_2WO_6 lamellas (L-BWO) are about 50 nm in length and 5–10 nm in thickness. As the pH value decreases to 4.0, the Bi_2WO_6 products have the unique flower-like (F-BWO) spherical superstructures which are made up of several nanolamellas (Fig. 1(b)). When pH 2.0, the Bi_2WO_6 sample exhibits

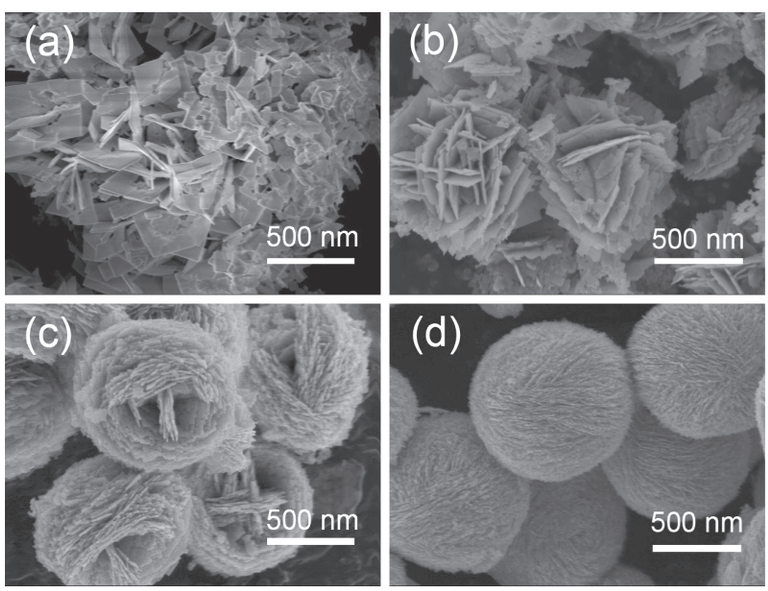

Fig. 1. FE-SEM images of Bi_2WO_6 products with different morphologies. (a) L-BWO, (b) F-BWO, (c) N-BWO, and (d) C-BWO.

a hierarchical system in which the nanolamellas are well-ordered and oriented to form a hollow nest-like (N-BWO) hierarchical structure (Fig. 1(c)). For the sample prepared at pH 0.5, caddice clew-like Bi_2WO_6 (C-BWO) spheres are obtained. The hierarchical spheres are convoluted by hundreds of nanolamellas and their average diameter is about 1 μm (Fig. 1(d)).

Figure 2 shows the XRD patterns of Bi_2WO_6 with different morphologies. Although their reaction pH values are different, the XRD patterns of the products present almost the same profiles. All the diffraction peaks correspond well with orthorhombic Bi_2WO_6 (JCPDS No.73-1126). No peaks due to impurities are detected, indicating that all bismuth salt precursors have been thoroughly decomposed into pure Bi_2WO_6 during the reaction.

Figure 3(a) displays the UV-vis diffuse reflectance spectra (DRS) of the Bi_2WO_6 samples with different morphologies. It can be seen that the Bi_2WO_6 products have similar DRS spectra. They all have a steep absorption edge in the visible light region, which suggests that the relevant band gap is due to the intrinsic transition of the nanomaterials rather than the transition from impurity levels. The bandgap (E_g) obtained by extrapolation of the plots (in the inset of Fig. 3(a)) are 2.76, 2.70, 2.61 and 2.68 eV for the L-BWO, F-BWO, N-BWO and C-BWO products, respectively. These results indicate that all these Bi_2WO_6 samples have a bandgap suitable for photocatalytic decomposition of organic contaminants under visible-light irradiation.

The nitrogen adsorption–desorption isotherms and pore size distributions of the Bi_2WO_6 products were further investigated in Figure 3(b). The nitrogen adsorption and desorption isotherms are characteristic of a type IV isotherm with a hysteresis loop, indicating the Bi_2WO_6 hierarchical structures are composed of connected mesopores.[17–18] The S_{BET} of catalysts are 16.3 m^2/g for L-BWO, 24.7 m^2/g for F-BWO, 39.4 m^2/g for N-BWO and 36.8 m^2/g for C-BWO, respectively. The optical properties, porous structure and large S_{BET} would endow the as-prepared Bi_2WO_6 products with potential application as effective photocatalyst.

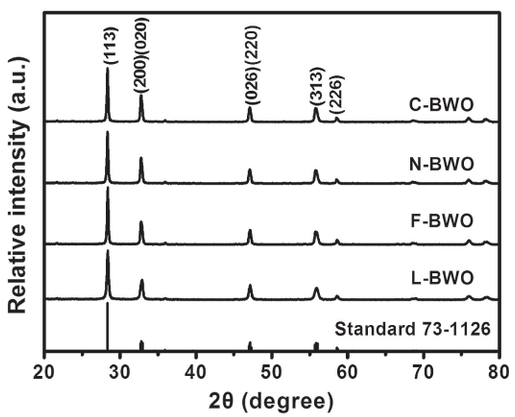

Fig. 2. XRD patterns of Bi_2WO_6 products with different morphologies.

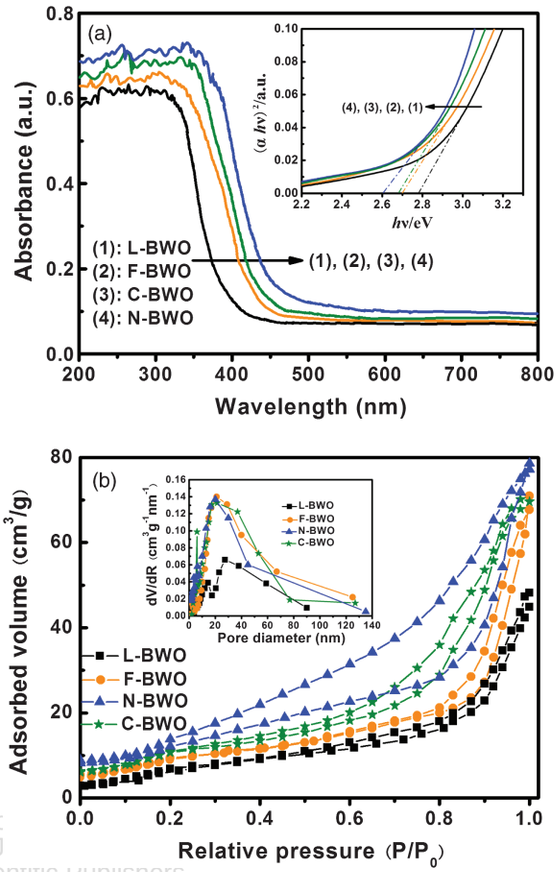

Fig. 3. (a) UV-Vis diffuse reflectance spectra of Bi_2WO_6 products with different morphologies. Inset is the correspondin plot of $(\alpha h\nu)^2$ versus photon enery ($h\nu$) for Bi_2WO_6 particles. (b) Nitrogen adsorption–desorption isotherms of Bi_2WO_6 products with different morphologies. Inset: Pore size distribution curve of the as-prepared samples.

3.2. Photocatalytic Performance

To evaluate the photocatalytic performance of Bi_2WO_6 products, a widely used dye, RhB was selected as the model pollutant. For comparison, the RhB photodegradation by the Degussa P25 was also performed under visible light. The results are shown in Figure 4(a). Blank test shows that no degradation of RhB in the absence of photocatalyst. There is a slight degradation of RhB over P25 in the given reaction period due to the dye-sensitive visible-light photocatalytic effect on the surface of P25. In contrast, significant degradation has been observed on the as-synthesized Bi_2WO_6 photocatalysts. Here, the N-BWO shows the best photodegradation rate of RhB, on which the RhB decomposition extent is nearly three times of L-BWO sample. The photocatalytic performance on C-BWO and F-BWO products are almost identical, but far lower than that of N-BWO sample. The lowest photocatalytic efficiency of L-BWO is probably due to its

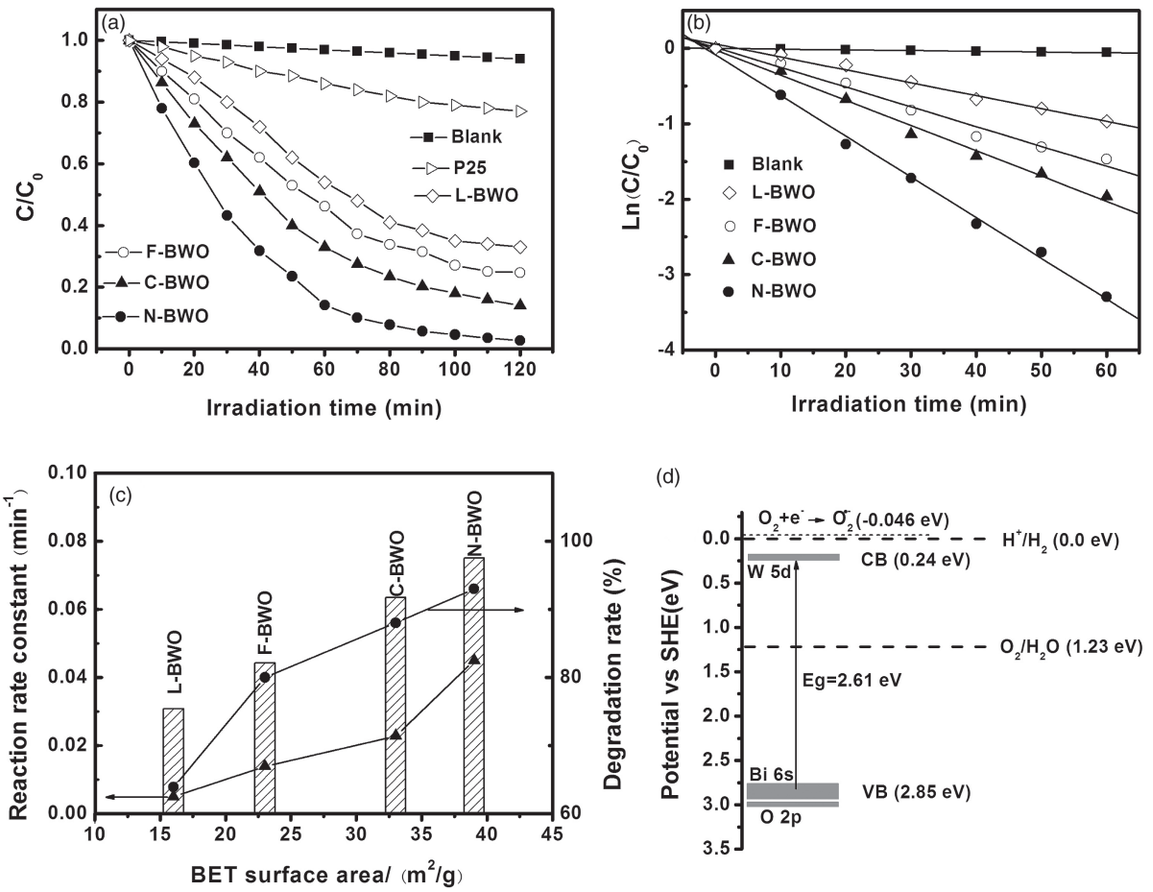

Fig. 4. (a) Photocatalytic degradation of RhB using as-prepared Bi_2WO_6 with different morphologies under visible-light irradiation. (b) Kinetic linear simulation curve of RhB photocatalytic degradation with different catalysts. (c) Relationship between reaction rate constant (-▲-), degradation rate (-●-), and BET surface area over Bi_2WO_6 products with different morphologies. (d) Schematic band structure of Bi_2WO_6.

relative higher band gap energy. As is known, the lower the band gap energy, the higher the visible-light energy absorbed to activate the photocatalyst;[19] accordingly, oxidation is enhanced, and degradation of organic compounds is accelerated. So, the highest band gap energy of L-BWO nanostructures related well to the lowest photodegradablity of RhB.

The difference in photocatalytic efficiency among the four hierarchical structures can be further illustrated with Figure 4(b), which shows the RhB degradation kinetics data. The photocatalytic degradation of RhB was described by the Langmuir-Hinshelwood (L-H) model which is well-established for photocatalysis experiments when the pollutant is in the millimolar concentration range.[20] The photocatalytic destruction of RhB was recognized to follow first-order reaction kinetics approximately, as evidenced by linear plot of ln (C/C_0) versus photocatalytic reaction time. Figure 4(c) shows the relationship between reaction rate constant, BET surface area and RhB degradation rate. The reaction rate constant of the N-BWO sample with 39.4 m^2/g BET surface area is estimated to be 0.053 min^{-1}, faster than those over C-BWO and F-BWO samples with lower BET surface areas. These results illustrate that the high surface area of Bi_2WO_6 is a key to the high rate constant, resulting a high RhB degradation rate. In addition, the N-BWO sample possesses the unique hollow hierarchical structure in which large numbers of mesopores can serve as efficient transport paths for the destruction of RhB.

3.3. Photocatalytic Mechanism

The conductance and valence band (CB and VB) edge electrochemical potentials of Bi_2WO_6 semiconductor are crucial factors to understand the photocatalytic mechanism of RhB over Bi_2WO_6 products. Figure 4(d) shows a schematic band structure of Bi_2WO_6 semiconductor based on the earlier calculation. Since the calculated VB edge potential of Bi_2WO_6 (+2.85 eV) is more positive than the standard redox potentials of $OH^{\cdot}/OH^{-}$ (+1.99 eV), indicating that the photogenerated holes are far more oxidative than the active oxygen species such as $OH^{\cdot}$ radicals. Meanwhile, the photoexcited holes on the surface of Bi_2WO_6 cannot oxidize OH^{-} to form the $OH^{\cdot}$ radicals due to the more negative reduction potential of Bi^{+5}/Bi^{+3} ($E^0 = +1.59$ eV at pH 0).[21] Therefore, it is theoretically

reasonable that direct photogenerated holes mainly govern the photocatalytic oxidation of RhB by Bi_2WO_6. In addition, the CB edge potential of Bi_2WO_6 (0.24 eV) is positive enough to reduce the O_2 molecule to the oxygen radical by the photoexcited electron due to the electrochemical potential for single-electron reduction of oxygen is −0.046 eV.[22] So the production of oxygen radical can prevent the recombination of the photoexcited electrons and holes and increase the photodegradation of RhB. The possible photocatalytic mechanism under visible light was proposed as follows:

$$Bi_2WO_6 + \text{visible light} \rightarrow Bi_2WO_6(e^-_{cb} + h^+_{vb}) \quad (1)$$

$$Bi_2WO_6(e^-_{cb}) + O_{2ads} \rightarrow Bi_2WO_6 + O^{\bullet -}_{2ads} \quad (2)$$

$$h^+_{vb},\ O^{\bullet -}_{2ads} + \text{RhB} \rightarrow \text{deg raded products} \quad (3)$$

Since the photocatalytic reactions take place on the surface of photocatalyst, the difference of structure and morphology certainly will affect the efficiency of photocatalytic reactions. The N-BWO sample possesses the unique hollow hierarchical structure in which large numbers of mesopores can serve as efficient transport paths for the destruction of RhB. Furthermore, the N-BWO sample has large surface area, which not only provides active sites for the degradations reaction, but also effectively promotes the separations of the electron–hole pairs, resulting in a higher quantum efficiency of photocatalytic reaction.

4. CONCLUSIONS

In summary, nanostructured Bi_2WO_6 with different hierarchical morphologies was synthesized via a facile hydrothermal route. The relationship between morphology and photocatalytic performance of the as prepared samples was discussed. Although all the Bi_2WO_6 products demonstrate photocatalytic activity to the decomposition of RhB under visible-light irradiation, the degradation over the N-BWO sample is more significantly efficient due to the effective visible absorption and the large surface area. All the results indicate that morphology plays an important role in the photocatalyitc property of Bi_2WO_6.

Acknowledgments: This work was financially supported by a grant from the Major State Basic Research Development Program of China (973 Program) (Grant No. 2007CB936601).

References and Notes

1. S. L. Fischer and C. P. Koshland, *Environ. Sci. Technol.* 41, 3121 (**2007**).
2. H. B. Fu, C. S. Pan, W. Q. Yao, Y. F. Zhu, *J. Phys. Chem. B* 109, 22432 (**2005**).
3. L. D. Zhang and M. Fang, *Nano Today* 5, 128 (**2010**).
4. Z. Jiang, F. Yang, G. D. Yang, L. Kong, M. O. Jones, T. C. Xiao, P. P. Edwards, *J. Photoch. Photobio. A* 212, 8 (**2010**).
5. G. S. Li, D. Q. Zhang, J. C. Yu, M. K. Leung, *Environ. Sci. Technol.* 44, 4276 (**2010**).
6. L. S. Zhang, W. Z. Wang, Z. G. Chen, and H. L. Xu, *Small* 3, 1618 (**2007**).
7. C. Zhang and Y. F. Zhu, *Chem. Mater.* 17, 3537 (**2005**).
8. J. Y. Xiang, J. P. Tu, L. Zhang, Y. Zhou, X. L. Wang, and S. J. Shi, *J. Power Sources* 195, 313 (**2010**).
9. M. Shang, W. Z. Wang, S. M. Sun, L. Zhou, and L. Zhang, *J. Phys. Chem. C* 112, 10407 (**2008**).
10. X. J. Dai, Y. S. Luo, W. D. Zhang, and S. Y. Fu, *Dalton Trans.* 39, 3426 (**2010**).
11. X. S. Fang, Y. Bando, U. K. Gautam, C. H. Ye, and D. Golberg, *J. Mater. Chem.* 18, 509 (**2008**).
12. W. Z. Yin, W. Z. Wang, and S. M. Sun, *Catal. Commun.* 11, 647 (**2010**).
13. X. S. Fang, T. Y. Zhai, U. K. Gautam, L. Li, L. M. Wu, Y. S. Bando, D. T. Golberg, *Prog. Mater. Sci.* 56, 175 (**2011**).
14. G. M. Hua, Y. Tian, L. L. Yin, and L. D. Zhang, *Cryst. Growth Des.* 9, 4653 (**2009**).
15. X. S. Fang, L. M. Wu, and L. F. Hu, *Adv. Mater.* 23, 585 (**2011**).
16. Y. Tian, G. M. Hua, W. Xu, N. Li, M. Fang, and L. D. Zhang, *J. Alloys. Compd.* 509, 724 (**2011**).
17. M. A. Butler, *J. Appl. Phys.* 48, 1914 (**1977**).
18. J. C. Yu, X. C. Wang, and X. Z. Fu, *Chem. Mater.* 16, 1523 (**2004**).
19. J. W. Tang, Z. G. Zou, and J. H. Ye, *Chem. Mater.* 16, 1644 (**2004**).
20. C. S. Turchi and D. F. Ollis, *J. Catal.* 122, 178 (**1990**).
21. H. B. Fu, C. S. Pan, L. W. Zhang, and Y. F. Zhu, *Mate. Res. Bull.* 42, 696 (**2007**).
22. D. Wang, T. Kako, and J. Ye, *J. Am. Chem. Soc.* 130, 2724 (**2008**).

Received: 4 January 2011. Accepted: 22 February 2011.

RESEARCH ARTICLE